The Journal of the Acoustical Society of America

MAY 09 2023

Experimental demonstration of low signal-to-noise ratio matched field processing with a geoacoustic model extracted from noise FREE

F. Hunter Akins ; W. A. Kuperman

J. Acoust. Soc. Am. 153, 2818 (2023)
https://doi.org/10.1121/10.0019377

JASA ARTICLE

Experimental demonstration of low signal-to-noise ratio matched field processing with a geoacoustic model extracted from noise

F. Hunter Akins[a)] and W. A. Kuperman
Scripps Institution of Oceanography, University of California, San Diego, La Jolla, California 92093-0701, USA

ABSTRACT:
Passive localization of a low signal-to-noise ratio (SNR) source in a shallow water waveguide without prior geoacoustic information is accomplished by combining the mode-extraction method modal-MUSIC (multiple signal classification) with range-coherent matched field processing (MFP). Range-coherent MFP coherently combines snapshots from different resolution cells to obtain gain over noise. Modal-MUSIC uses knowledge of the water column sound speed profile (no bottom information) to extract noisy estimates of modal wavenumbers from ship noise recorded on a partially spanning vertical line array (VLA). A geoacoustic model is then fit to the wavenumber estimates extracted from noise with modal-MUSIC and used to compute replicas for range-coherent MFP. The combination of these two methods applied to a 21-element VLA achieves successful source localization at SNR levels as low as -20 dB using ten tonals transmitted during the SWellEx96 experiment.
https://doi.org/10.1121/10.0019377

(Received 24 February 2023; revised 14 April 2023; accepted 23 April 2023; published online 9 May 2023)

[Editor: Julien Bonnel] Pages: 2818–2825

I. INTRODUCTION

Matched field processing (MFP) passively localizes a source by comparing the acoustic field measured on an array to modeled fields for various candidate source positions. To successfully localize a source, MFP requires an accurate environmental model, which, at low frequency in shallow water, includes information about propagation characteristics in the seabed. The challenges of obtaining such a model limit the applicability of MFP. By passively extracting the geoacoustic portion of the environmental model from ambient noise, this work successfully applies MFP in the absence of comprehensive *a priori* environmental knowledge.

Geoacoustic parameters can be extracted from various acoustic observables, such as: modal group speed,[1] noise correlations between vertically separated sensors,[2] the power reflection coefficient,[3] complex pressure field measured at known ranges,[4] noise from a ship of opportunity recorded on a horizontal line array (HLA),[5] sound from a ship of opportunity of known position,[6] noise from a ship of opportunity inverted using a matched field inversion,[7,8] noise with a full water column spanning array,[9] echosounder measurements, and so on. This work is concerned with passive localization in a (partially) unknown environment. Therefore, estimation of an unknown environment from acoustic data must be carried out without the benefit of an active source. For the experimental scenario of interest, the real parts of the wavenumbers of the modal field are extracted from the covariance matrix of noise in the band from 50 Hz to 250 Hz on a partially spanning vertical line array (VLA) using modal-MUSIC (multiple signal classification).[10] The estimated wavenumbers yield information on the sediment compressional sound speed, density, and layer thickness, but do not contain direct information on sediment attenuation. However, modal-MUSIC also estimates the number of modes present in the field, which can be used for accurate replica calculation in the absence of sediment attenuation.[11] Geoacoustic parameters could also be included in the MFP search space such as in focalization.[12–14] However, focalization greatly increases the computational demands of MFP and has never been experimentally demonstrated at low-SNR. Therefore, passive acquisition of a geoacoustic model from shipping noise is a useful step towards successful localization of a quiet source with MFP.

Once equipped with a sufficiently accurate model to perform MFP, localization of a quiet moving signal is still limited by coherent integration time and array gain. A moving source remains within a resolution cell for a finite time, which limits covariance matrix estimation. A recent method, "range-coherent MFP,"[15] coherently compares snapshots from separate resolution cells by modeling the effect of candidate source motions on the snapshots and comparing them with the data, with the caveat that the source frequency is known. Range-coherent MFP essentially allows one to add additional synthetic array staves to obtain array gain at the price of additional computation.

In this work, range-coherent MFP is used to localize a quiet source (frequency averaged SNR of -20 dB over ten tonals) at ranges out to 8 km using a 21-element vertical line

[a)]Electronic mail: fakins@ucsd.edu

array (VLA). The replicas used for MFP are computed using a geoacoustic model extracted from shipping noise using modal-MUSIC. Therefore, a single system can both obtain the geoacoustic information necessary for localization and carry out the localization.

II. MODAL-MUSIC

Modal-MUSIC is an array processing method that combines the MUSIC algorithm[16] with the shooting method[17] to extract normal modes from shipping noise using a VLA.[10]

Under certain conditions,[10] (1) the eigenvectors of the covariance matrix of the array can be partitioned into signal and noise subspaces and (2) candidate normal modes that are orthogonal to the noise subspace are the true modes of the waveguide. The modal-MUSIC spectrum is then defined as

$$P_{moMU}(k_r) = \left[\boldsymbol{\Phi}(k_r)\boldsymbol{E}_N\boldsymbol{E}_N^{\dagger}\boldsymbol{\Phi}(k_r)\right]^{-1}, \tag{1}$$

where $\boldsymbol{\Phi}(k_r)$ is the mode shape associated with candidate wavenumber k_r, sampled at the array elements, obtained by the shooting method using the water column sound speed profile (SSP). The columns of the matrix $\boldsymbol{E}_N$ are the eigenvectors of the sample covariance matrix (SCM) associated with the noise subspace.

In order to compare the spectra at different frequencies, it is convenient to introduce a "mode angle," which is defined as

$$\theta \equiv \arccos(k_r/(\omega/c_{\min})), \tag{2}$$

where $\omega = 2\pi f$ is the frequency under consideration and c_{min} is the minimum value of the SSP.

III. GEOACOUSTIC INFORMATION IN THE MODAL-MUSIC SPECTRUM

This section discusses the extraction of a geoacoustic model from modal-MUSIC wavenumber estimates and presents relevant uncertainty analysis for the model fit. In previous work,[10] wavenumber estimates were de-noised by fitting polynomials to the identified modes in the dispersion curve. These polynomials produced sufficiently accurate wavenumber estimates to localize a loud source to around 5 km but failed to localize at greater range or to localize a quiet source. The failure is believed to be due to poor estimation of low-order modes, which will be improved by fitting a geoacoustic model to high order modes. In particular, simulations demonstrate that the high-order modes will be estimated with lower variance than low order modes. This is fortuitous for geoacoustic model fit, as the high-order modes contain more geoacoustic information than low-order modes.

Once modes have been identified in the modal-MUSIC dispersion curve, a misfit function between model and data may be defined as follows:

$$J(\boldsymbol{x}) = \sum_{i=1}^{N_f}\sum_{j\in M_i}(\hat{k}_j(f_i) - k_j(f_i;\boldsymbol{x}))^2/\sigma_{ij}^2, \tag{3}$$

where $\hat{k}_j(f_i)$ is the estimate of the jth mode wavenumber at frequency f_i with error variance σ_{ij}^2, M_i is the set of well-estimated modes at frequency f_i, N_f is the number of frequencies at which modal-MUSIC was performed, and $k_j(f_i;\boldsymbol{x})$ is the forward model calculation of the jth mode at frequency f_i for bottom parameters $\boldsymbol{x}$. The minimum of this function $\boldsymbol{x}_*$ corresponds to the best model fit.

In addition to mode-dependent estimate error variance σ_{ij}^2, there is also a mode-specific model sensitivity. Modes with a phase speed less than the sediment sound speed have an exponentially decaying tail in the bottom, and the horizontal wavenumber is relatively insensitive to bottom parameters[19] compared to modes that are oscillating in the sediment. In Sec. III A, Monte Carlo simulations will show that *the modes which are most sensitive to the properties of the sediment are also the modes that can be estimated with the least variance*.

A. Monte Carlo simulations for uncertainty demonstration

Monte Carlo simulations are carried out to demonstrate modal-MUSIC uncertainty under ideal conditions over a range of frequencies. The simulations use the environmental model and array geometry shown in Fig. 1, which parallel the SWellEx-96 experiment setup.

Each snapshot realization, expressed as a vector, is

$$\boldsymbol{p}_i = \sum_{m=1}^{M} x_m^i \Phi_m(\boldsymbol{z}) + \boldsymbol{n}_i, \tag{4}$$

where $x_m^i \sim \mathcal{N}(0, \Phi_m(z_s)^2)$ is a random Gaussian amplitude with variance equal to the mode excitation strength for a source depth at 10 m (chosen to be characteristic of a ship), $\Phi_m(\boldsymbol{z})$ is the mth mode evaluated at the array depths in vector $\boldsymbol{z}$, M is the number of modes, and $n_i \sim \mathcal{N}(0, \sigma_n^2 I)$ is zero-mean Gaussian noise. The diagonal value σ_n^2 of the noise covariance is selected to give an average single-sensor "SNR" of 20 dB. Here, SNR refers to the ratio of the variance of the modal component of the noise to the variance of the white noise component.

Then, an ensemble of 1000 snapshot realizations was used to form a single realization of the array sample covariance matrix (SCM)

$$\hat{K} = \frac{1}{1000}\sum_{i=1}^{1000}(\boldsymbol{p}_i - \hat{\boldsymbol{\mu}})(\boldsymbol{p}_i - \hat{\boldsymbol{\mu}})^{\dagger}, \tag{5}$$

where $\hat{\boldsymbol{\mu}}$ is the sample mean and $(\cdot)^{\dagger}$ denotes the conjugate transpose. For simulation, the number of modes is assumed to be known and is used to partition the eigenvectors of the SCM into the signal and noise subspaces. Finally, the noise

https://doi.org/10.1121/10.0019377

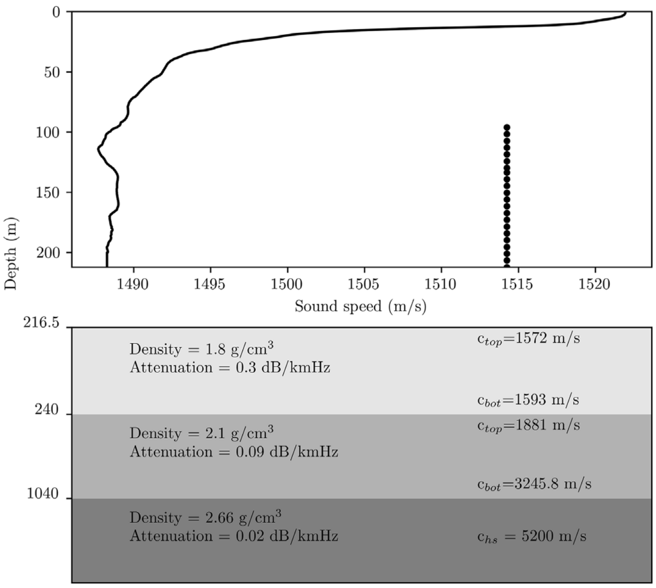

FIG. 1. Array and environmental model used for Monte Carlo simulations. The SSP comes from a CTD cast during the SWellEx96 experiment and is also used for modal-MUSIC in data processing. The array geometry is also representative of that used during the SWellEx96-experiment, consisting of a 21 element array spanning approximately 120 m. The geoacoustic model is due to Bachman (Ref. 18) and is used for conventional MFP in this work. The SSP shown is also used for the shooting method for modal-MUSIC.

subspace estimated this way is used to compute a modal-MUSIC spectrum using Eq. (1).

100 SCM realizations are used to obtain 100 realizations of the modal-MUSIC spectrum. From this ensemble, means and variances are estimated for each mode at each frequency. The results are shown in Fig. 2 and indicate that, for the SWellEx-96 experiment at 20 dB SNR with 1000 snapshots, modal-MUSIC should estimate the low-order modes with high error variance but should estimate the higher-order modes accurately. Figure 2 also includes a red box indicating the modes that are both sensitive to bottom properties and estimated with low variance.

B. Number of propagating modes: Cutoff modal angle

Attenuation is an important geoacoustic parameter for low-frequency shallow water MFP replicas. Baxley *et al.*[11] show that, within a certain source radius, the main effect of bottom attenuation on MFP replicas is the determination of the effective mode cutoff in the modal sum. That is, the attenuation determines the *number* of propagating modes, while the effect of attenuation on relative modal amplitudes within the set of propagating modes is relatively small.

For example, consider the Bachman geoacoustic model (Fig. 1) for the SWellEx experimental region.[18] It has a half-space compressional speed of 5200 m/s, meaning that, in the absence of attenuation, there are *propagating* modes with a modal angle up to 73°. The presence of sediment attenuation adds a significant imaginary part to the modal wavenumbers above a certain frequency-dependent cutoff mode angle $\theta_c(f)$ (an effective "modal critical angle"), so the modes with $\theta(k_r) > \theta_c(f)$ are stripped from the waveguide after a short range. However, the sediment attenuation is still low enough to allow modes below this modal critical angle to significantly affect the replicas out to a range of 10 km. An approximation to the replicas that uses the real part of the wavenumbers and an accurate, frequency-dependent modal critical angle will provide good agreement with data from within a certain radius.

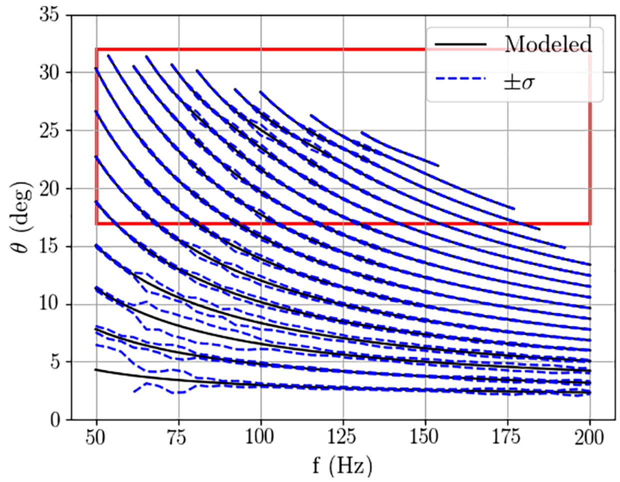

FIG. 2. (Color online) Monte Carlo simulation results demonstrating uncertainty in the modal-MUSIC spectrum. One standard deviation is shown as blue dashed lines bracketing the real modes shown as black lines from 100 realizations of the SCM for a modal matrix with a source at 10 m depth and no correlation between modes. The red box emphasizes a region of the dispersion curve that (a) is well-estimated by modal-MUSIC and (b) is sensitive to the geoacoustic properties.

Modal-MUSIC only produces estimates of the real part of the wavenumbers, and therefore carries no precise information on the sediment attenuation. Examination of the modal-MUSIC spectrum on data (for example, see Fig. 3) suggests that modal-MUSIC may provide a good estimate $\hat{\theta}_c(f)$ of the modal cutoff angle. The compressional speed, density, and layer properties of the geoacoustic model can

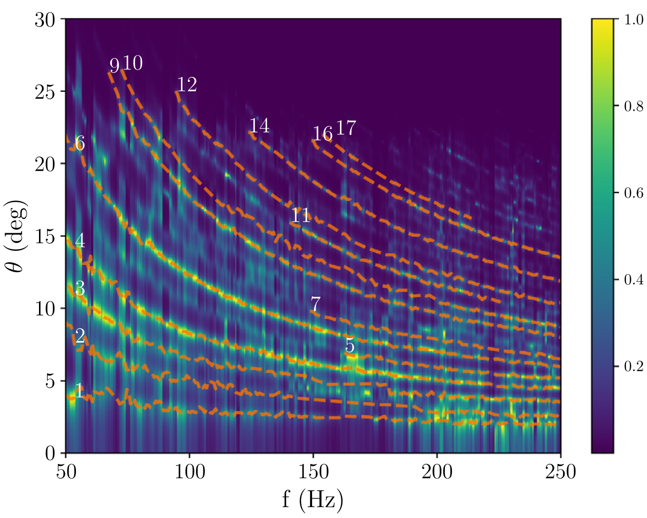

FIG. 3. (Color online) Normalized modal dispersion curve from modal-MUSIC with identified modes superimposed as orange dashed lines and labeled with white text.

be fit to the modal-MUSIC spectrum, and then this model can be augmented with $\hat{\theta}_c(f)$. Together, these provide a reasonably accurate description of sound propagation in the shallow water waveguide without the need to explicitly include model attenuation.

The cutoff angle $\theta_c(f)$ is estimated at a given frequency by picking the highest angle peak with a normalized amplitude above a threshold value of 0.1. The collection of highest angle peaks, smoothed with a five-point median filter over frequency, provides the cutoff angle $\hat{\theta}_c(f)$ used for MFP.

IV. RANGE-COHERENT MATCHED FIELD PROCESSING

By modeling source motion, range-coherent MFP[15] coherently combines snapshots from a moving source crossing multiple resolution cells. This section introduces notation necessary to present results in the following.

Consider a sequence of L snapshots taken at a frequency f. At each time t_i, the source range and depth are r_i and z_i. Then the snapshot at time t_i is written as

$$\boldsymbol{d}_i = S_i(f)\boldsymbol{p}(r_i, z_i) + \boldsymbol{n}_i, \tag{6}$$

where $\boldsymbol{n}_i$ is noise from the sensors, interferers, etc., $\boldsymbol{p}$ is the pressure field due to the source and $S_i(f)$ is the complex source spectrum at frequency f. For a perfectly narrowband source, $S_i(f) = Ae^{j2\pi f t_i}$, with A equal to the complex value $S_0(f)$ at $t=0$.

Range-coherent MFP first removes the source phase from each snapshot to get a new sequence of measurements

$$\boldsymbol{d}'_i = \boldsymbol{d}_i e^{-j2\pi f t_i} = A\boldsymbol{p}(r_i, z_i) + \boldsymbol{n}'_i. \tag{7}$$

If the source is truly coherent and the frequency f is correctly specified, the effect of this correction is to (a) add a phase shift to the noise and (b) remove the effect of time on the phase of the pressure field due to the source. The leftover change in the pressure field is due only to change in source position and can therefore be modeled.

For a candidate source track $\{r_i, z_i\}$, the model produces a sequence $\{\boldsymbol{p}(r_i, z_i)\}$. Both the snapshot set $\{\boldsymbol{d}'_i\}$ and modeled set $\{\boldsymbol{p}(r_i, z_i)\}$ are stacked into "supervectors"

$$\boldsymbol{d}_{sup} = \left[\boldsymbol{d}_0'^T \boldsymbol{d}_1'^T \cdots \boldsymbol{d}_{L-1}'^T\right]^T \tag{8}$$

and

$$\boldsymbol{p}_{sup}(\{r_i, z_i\}) = \left[\boldsymbol{p}_0^T(r_0, z_0) \cdots \boldsymbol{p}_{L-1}^T(r_{L-1}, z_{L-1})\right]^T, \tag{9}$$

with L denoting the number of snapshots to be coherently combined.

In the case of a source moving at a constant depth and a constant range-rate, source position can be modeled using three parameters: constant depth z, initial range r_0 at initial time $t=0$, and constant range-rate $\dot{r}$. Multiple realizations of $\boldsymbol{d}_{sup}$ can be used to form a "super-covariance matrix":

$$\hat{\boldsymbol{K}} = \frac{1}{N_s}\sum_{i=1}^{N_s}(\boldsymbol{d}_{sup}^{(i)} - \hat{\boldsymbol{\mu}})(\boldsymbol{d}_{sup}^{(i)} - \hat{\boldsymbol{\mu}})^\dagger \tag{10}$$

($\hat{\boldsymbol{\mu}}$ is the sample mean). The Bartlett ambiguity surface is then computed as

$$B(r_0, z, \dot{r}, f) = \frac{\boldsymbol{p}_{sup}(r_0, z, \dot{r}, f)^\dagger \hat{\boldsymbol{K}} \boldsymbol{p}_{sup}(r_0, z, \dot{r}, f)}{||\boldsymbol{p}_{sup}(r_0, z, \dot{r}, f)||^2 \mathrm{tr}(\hat{\boldsymbol{K}})}, \tag{11}$$

where $\mathrm{tr}(\cdot)$ is the trace operation.

When multiple tonals are available, the ambiguity surfaces from each frequency are averaged in decibels,[20]

$$B(r_0, z, \dot{r}) = \frac{1}{N_f}\sum_{k=1}^{N_f} 10\log_{10} B(r_0, z, \dot{r}, f_k). \tag{12}$$

Finally, the source depth, range and range-rate are estimated as the values $r_0, z,$ and $\dot{r}$ that maximize the function (12).

For purposes of comparison, the range-coherent processor in Eq. (12) can be computed without applying the source phase correction in Eq. (7), yielding a "range-incoherent" matched field processor which performs similarly to matched field tracking.[21] The improvement of range-coherent over range-incoherent MFP is then attributable to coherent gain from combining snapshots from separate resolution cells, as opposed to tracking gain from incoherently combining conventional MFP surfaces.

V. EXPERIMENTAL RESULTS: MODAL-MUSIC AND MODEL FIT

This section details the application of modal-MUSIC and geoacoustic model fitting to experimental data collected during the SWellEx96 experiment.[22] These results are shown in Fig. 5.

A. Modal-MUSIC dispersion curve

Modal-MUSIC is applied to a 30 min segment of data from JD131 2232 GMT to 2302 GMT, collected on 21 elements from the VLA. The first element is at a depth of 96 m, and the total array length is around 118 m. One element malfunctioned in a 22 element array with a uniform spacing of 5.625 m. The remaining 21 elements used for modal-MUSIC have a spacing of 5.625 m except for the two elements that bracketed the malfunctioning element, which are separated by 11.25 m. The dominant source of noise during this portion of data is thought to be from the research vessel transiting at ranges from approximately 8 to 10 km.

Each element samples the pressure field at a 1500 Hz sampling rate. To extract the modal-MUSIC dispersion curve, snapshots at frequencies from 50 to 250 Hz are formed using a 2048 point FFT (1.36 s length) with a Hamming window, with no overlap between snapshots. This results in 1318 snapshots used to form each frequency SCM (frequency spacing of 0.73 Hz).

https://doi.org/10.1121/10.0019377
JASA

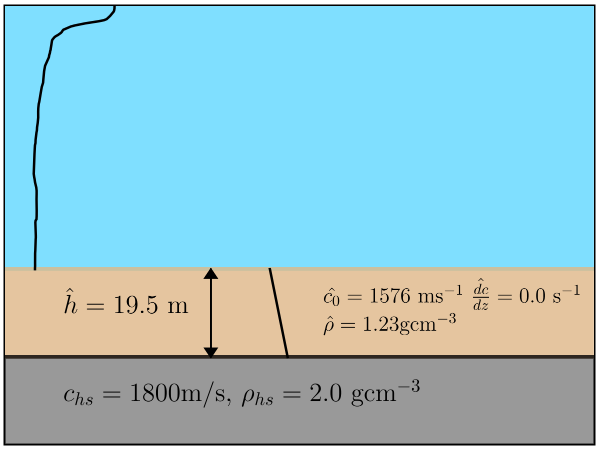

FIG. 4. (Color online) Single layer model (not to scale) fit to the modal-MUSIC dispersion curve. This model, along with the modal cutoff angle shown in Fig. 5, is used for range-coherent MFP results.

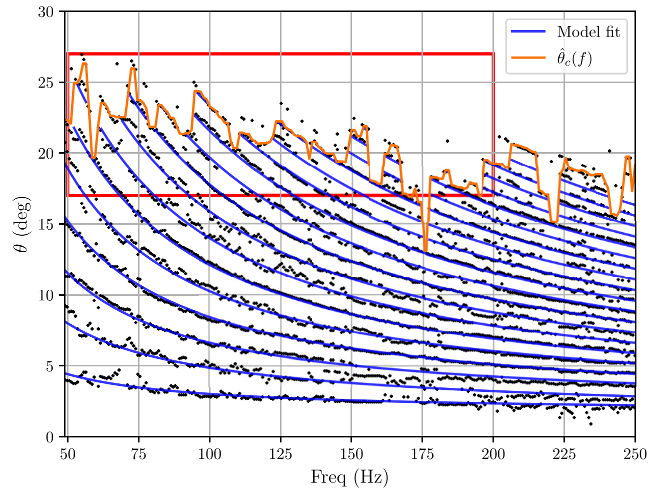

FIG. 5. (Color online) Results of performing the geoacoustic fit to modal-MUSIC spectrum. Wavenumbers used for geoacoustic model fit are shown in the red box. The blue lines show the forward model with the optimized dispersion curve. Peaks in the modal-MUSIC spectrum (see Fig. 3) with a normalized amplitude greater than 0.1 are shown as black dots. The orange dashed line shows the mode angle cutoff used in replica calculation for MFP as a function of frequency.

To compute the modal-MUSIC spectrum [Eq. (1)], the eigenvector decomposition of each SCM is computed, and the signal subspace rank at each frequency is estimated by looking for the maximum in the eigenvalue difference. Specifically, for eigenvalues sorted in decreasing order, the signal subspace dimension is defined as argmax $\{(\lambda_i - \lambda_{i+1})\}$ for $i = 1, 2, \ldots, 20$. Outliers are identified as spikes of magnitude greater than three in the subspace dimension estimate between adjacent frequencies. The outliers are removed, and then the subspace dimension estimates are smoothed over frequency by fitting them by a quadratic function.

The smoothed subspace estimates are used to estimate the noise subspace matrix $\boldsymbol{E}_N$. A CTD from a nearby time in the experiment (depicted in Fig. 1) is used for shooting candidate modes over the array.

Modes are then manually identified as smooth lines over frequency connecting the peaks in the dispersion curve. Figure 3 shows the modal-MUSIC spectrum as a function of frequency and mode angle θ_m with the identified modes, labeled. As seen in the figure, modes up to mode number 17 are identified in the dispersion curve.

B. Geoacoustic model fit

The emphasis here is to find a model that fits the modal-MUSIC curve well enough to perform MFP, rather than to find accurate estimates of the geoacoustic parameters with uncertainty quantification.

Precise mode estimate uncertainty cannot be known *a priori* since it depends on the (unknown) geoacoustic properties of the waveguide. However, the uncertainty analysis detailed in Sec. III A shows that the estimate error variance is roughly constant for estimated modes with a phase speed greater than or equal to 1550 m/s ($\approx 16^\circ$ mode angle), independent of frequency and mode number (see red box in Fig. 5). Furthermore, the objective function in Eq. (3) is insensitive to modes below this phase speed cutoff. Therefore, the geoacoustic fit is carried out using the wavenumber estimates of modes above this phase speed cutoff and assuming a constant error variance for those estimates. The presented results are insensitive to the precise choice of the cutoff phase speed.

The geoacoustic model consists of a single layer with constant density and linear SSP overlying a halfspace, as shown in Fig. 4. The four parameters in the layer include the

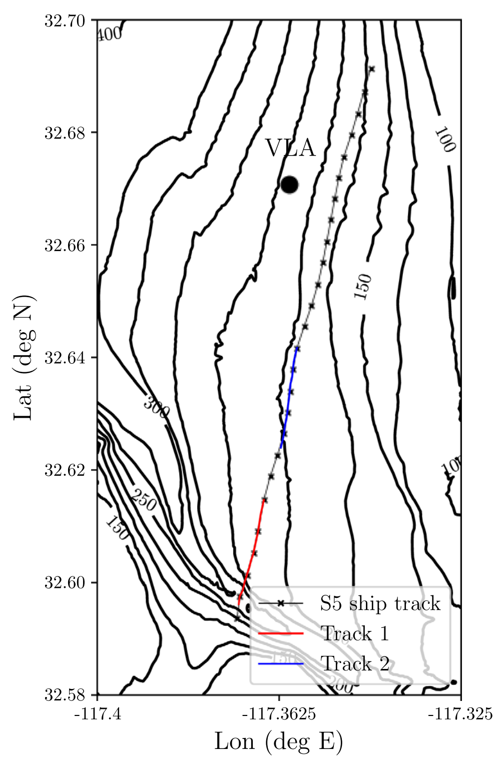

FIG. 6. (Color online) Bathymetry and source position during the S5 event of the SWellEx96 experiment.

JASA
https://doi.org/10.1121/10.0019377

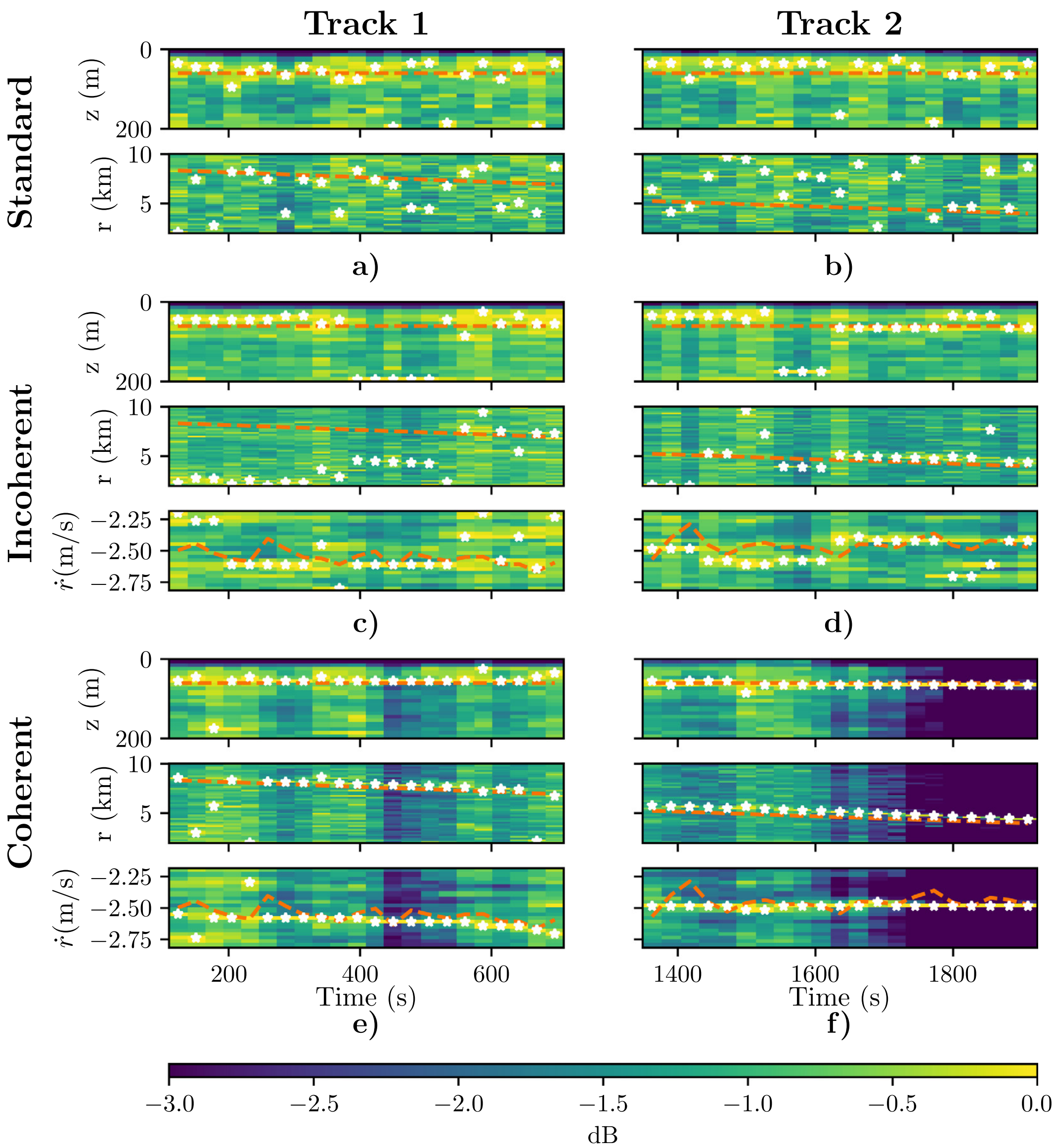

FIG. 7. (Color online) Comparison between [(a), (b)] conventional MFP, [(c), (d)] range-incoherent MFP, and [(e), (f)] range-coherent MFP. White stars mark the location of ambiguity surface maximum at each time. Orange dashed lines trace the source values, as determined by nominal depth, ship GPS, and Doppler estimates from the loud source tonals. The left column (a), (c), and (e) correspond to Track 1. The right column (b), (d), and (f) correspond to Track 2. Color scale is the value of Bartlett processor [Eq. (12)] in decibels, normalized to maximum beamformer output at each covariance integration period. Range-incoherent and range-coherent MFP also include a range-rate vs time ambiguity surface.

layer width h, the compressional speed at the top of the layer c_0, the sound speed gradient in the layer $s = dc/dz$, and the layer density ρ assumed to be constant. The dispersion curve is insensitive to the halfspace parameters, as long as the compressional speed in the halfspace is high enough to support all the estimated modes. The maximum observed phase speed is 1750 m/s in Fig. 3, so the halfspace speed is fixed arbitrarily at 1800 m/s and the density at $2\,\mathrm{g\,cm^{-3}}$ for the optimization.

Equipped with this model parameterization, the optimal parameter vector $\boldsymbol{x} = [h\ c_0\ s\ \rho]^T$ is found by minimizing the objective function in Eq. (3). The layer thickness is constrained to lie between 5 and 100 m, the compressional speed between 1540 and 1800 m/s, the gradient between 0 and $4\,\mathrm{s^{-1}}$, and density between 1.2 and $2.0\,\mathrm{g\,cm^{-3}}$. Wavenumbers for each candidate parameter vector $\boldsymbol{x}$ were computed using the Sturm sequence eigenvalue search[23] (the method used in KRAKEN[24]) The objective function is minimized by performing a sequential 1D optimization over each parameter, holding the others fixed at their latest optimized value. Six iterations were seen to provide good convergence. An optimal value of $\boldsymbol{x}_* = [19.5\,\mathrm{m}, 1576\,\mathrm{m/s}, 0\,\mathrm{s^{-1}}, 1.23\,\mathrm{g\,cm^{-3}}]^T$ was consistently found for several different choices for the initial parameter values. The wavenumbers from the optimized model are shown superimposed over the modal-MUSIC spectrum in Fig. 5. The phase speed of the highest angle estimated mode is used as a phase speed cutoff for each frequency when calculating replicas.

VI. EXPERIMENTAL RESULTS: RANGE-COHERENT MATCHED FIELD PROCESSING

This section details the localization of a quiet towed source using range-coherent MFP with the modal-MUSIC-derived model replicas described in Sec. V. These results are compared to traditional MFP using replicas computed from the geoacoustic model shown in Fig. 1. An additional comparison is made to range-incoherent MFP, where range-coherent MFP is carried out without correcting the source phase as in Eq. (7). The incoherent approach will average down sidelobes that move at a different speed from the candidate search speed but will not get the coherent gain over noise from coherent snapshot comparison.

A. S5 event

The S5 event of the SWellEx96-experiment consists of a roughly straight source tow during a 75 min period. During this time, a source towed at roughly 60 m depth played five tonal sets each consisting of 13 tonals between 49 and 400 Hz. Ten tones from the second tonal set, from 52 to 238 Hz, are used for testing localization results. From the 75 min event, two segments labeled “Track 1” and “Track 2” are selected for analysis. The source track during the event and these segments is shown in Fig. 6, and includes source ranges from 8 to 4 km.

Snapshots are formed by taking a 16 384-point Hamming-windowed FFT with a 50% overlap (5.46 s spacing). To simplify the presentation, prior knowledge of source range-rate was used to calculate the approximate Doppler-shifted signal bin from nominal frequency. Note that bin selection can be easily incorporated into range-coherent MFP since it searches over range-rate. The snapshot length results in an estimated mean SNR of -20 dB over the first ten quiet source tones at a source range of 8 km and -12 dB at 5 km source range.

Resolution cell size is roughly 60 m for a 400 Hz source, corresponding to a 25 s integration time for a source moving 2.5 m/s. For a traditional MFP benchmark, five snapshots are used to form covariance matrices at the ten frequencies. Supervectors for range-incoherent and range-coherent MFP are formed by stacking ten snapshots, each separated by 27 s. This draws each snapshot in the supervector from a separate resolution cell. Then, five realizations of the supervector are formed by using five consecutive snapshots for the first snapshot in the supervector. These five realizations are averaged to form a “super” covariance matrix of dimension 210×210 (21 real vertical array elements times 10 synthetic horizontal elements).

The covariance matrices are then used to evaluate the Bartlett ambiguity surface on a grid of source range, depth and, for range-coherent and range-incoherent MFP, range-rate. For traditional MFP, this yields a 3D surface over time, range, and depth. For range-coherent/“incoherent” MFP, it yields a 4D surface over time, range, depth, and range-rate. To visualize these results, 2D surfaces are formed by holding two axes fixed and taking the maximum over the other axis/axes. For example, a depth-time ambiguity surface for range-coherent MFP results can be formed by taking the maximum over all ranges and range-rates for each fixed covariance time and depth.

The results are shown in Fig. 7. For the quiet tonal set, conventional MFP is unable to localize the source for either of the two segments. Range-incoherent MFP produces some weak estimates out to a range of around 5 km before breaking down. Range-coherent MFP with the modal-MUSIC derived replicas successfully localizes the source out to a range of 8 km (estimated SNR of -20 dB).

VII. CONCLUSION

This work presents an approach for localizing a quiet coherent source using geoacoustic information extracted from the noise field. This method requires knowledge of the water-column SSP. Relevant geoacoustic information is extracted from noise using modal-MUSIC. The noise field is thought to be comprised mostly of shipping noise, given the calm sea state and common ship activity in the region. The extracted geoacoustic information is used to compute replicas for range-coherent MFP, which successfully localizes a multi-tone source at -20 dB SNR.

In this work, range-coherent MFP manages to extract gain by coherently comparing data from resolution cells that are separated by five minutes, or more than 800 m in range. This is perhaps surprising, given that the source motion is not perfectly uniform during this interval and the replicas are not perfectly matched to the environment. The successful localization results at low SNR presented here suggest that the phase evolution in range of the modal field may be a quantity robust to both non-uniform motion and replica mismatch, although further research is needed to explore this theoretically.

The contribution of modal-MUSIC is to provide both parameter estimates for a simple geoacoustic model, as well as estimates of a frequency-dependent, modal cutoff angle $\hat{\theta}_c(f)$. The use of a model improves localization results over the purely data-based approach used in previous work.[10] This improvement is likely due to the reduction of error in the low-order modes, which should be well constrained by the SSP (which is presumed known) but are poorly estimated by modal-MUSIC. Therefore, the model fit ensures a physically consistent set of modes, which improves the replica accuracy.

ACKNOWLEDGMENTS

This work was funded by the TFO program of the United States Office of Naval Research. Bill Hodgkiss and Dave Ensberg helped with data access for the SWellEx-96 experiment.

[1] J. Bonnel, Y.-T. Lin, D. Eleftherakis, J. A. Goff, S. Dosso, R. Chapman, J. H. Miller, and G. R. Potty, “Geoacoustic inversion on the New England mud patch using warping and dispersion curves of high-order modes,” J. Acoust. Soc. Am. **143**(5), EL405–EL411 (2018).

[2]M. Siderius, C. H. Harrison, and M. B. Porter, "A passive fathometer technique for imaging seabed layering using ambient noise," J. Acoust. Soc. Am. **120**(3), 1315–1323 (2006).
[3]C. H. Harrison and D. G. Simons, "Geoacoustic inversion of ambient noise: A simple method," J. Acoust. Soc. Am. **112**(4), 1377–1389 (2002).
[4]G. V. Frisk, K. M. Becker, S. D. Rajan, C. J. Sellers, K. von der Heydt, C. M. Smith, and M. S. Ballard, "Modal mapping experiment and geoacoustic inversion using sonobuoys," IEEE J. Oceanic Eng. **40**(3), 607–620 (2015).
[5]K. D. Heaney, "Rapid geoacoustic characterization using a surface ship of opportunity," IEEE J. Oceanic Eng. **29**(1), 88–99 (2004).
[6]C. Park, W. Seong, and P. Gerstoft, "Geoacoustic inversion in time domain using ship of opportunity noise recorded on a horizontal towed array," J. Acoust. Soc. Am. **117**(4), 1933–1941 (2005).
[7]M. Nicholas, J. S. Perkins, G. J. Orris, L. T. Fialkowski, and G. J. Heard, "Environmental inversion and matched-field tracking with a surface ship and an L-shaped receiver array," J. Acoust. Soc. Am. **116**(5), 2891–2901 (2004).
[8]D. Tollefsen and S. E. Dosso, "Bayesian geoacoustic inversion of ship noise on a horizontal array," J. Acoust. Soc. Am. **124**(2), 788–795 (2008).
[9]T. B. Neilsen and E. K. Westwood, "Extraction of acoustic normal mode depth functions using vertical line array data," J. Acoust. Soc. Am. **111**(2), 748–756 (2002).
[10]F. H. Akins and W. A. Kuperman, "Modal-MUSIC: A passive mode estimation algorithm for partially spanning arrays," JASA Express Lett. **2**(7), 074802 (2022).
[11]P. A. Baxley, N. O. Booth, and W. S. Hodgkiss, "Matched-field replica model optimization and bottom property inversion in shallow water," J. Acoust. Soc. Am. **107**(3), 1301–1323 (2000).
[12]M. D. Collins and W. A. Kuperman, "Focalization: Environmental focusing and source localization," J. Acoust. Soc. Am. **90**(3), 1410–1422 (1991).
[13]S. E. Dosso and M. J. Wilmut, "Bayesian focalization: Quantifying source localization with environmental uncertainty," J. Acoust. Soc. Am. **121**(5), 2567–2574 (2007).
[14]A. M. Thode, G. L. D'Spain, and W. A. Kuperman, "Matched-field processing, geoacoustic inversion, and source signature recovery of blue whale vocalizations," J. Acoust. Soc. Am. **107**(3), 1286–1300 (2000).
[15]F. Hunter Akins and W. A. Kuperman, "Range-coherent matched field processing for low signal-to-noise ratio localization," J. Acoust. Soc. Am. **150**(1), 270–280 (2021).
[16]R. Schmidt, "Multiple emitter location and signal parameter estimation," IEEE Trans. Antennas Propag. **34**(3), 276–280 (1986).
[17]M. B. Porter and E. L. Reiss, "A note on the relationship between finite-difference and shooting methods for ODE eigenvalue problems," SIAM J. Numer. Anal. **23**(5), 1034–1039 (1986).
[18]R. T. Bachman, P. W. Schey, N. O. Booth, and F. J. Ryan, "Geoacoustic databases for matched-field processing: Preliminary results in shallow water off San Diego, California," J. Acoust. Soc. Am. **99**(4), 2077–2085 (1996).
[19]S. D. Rajan, J. F. Lynch, and G. V. Frisk, "Perturbative inversion methods for obtaining bottom geoacoustic parameters in shallow water," J. Acoust. Soc. Am. **82**(3), 998–1017 (1987).
[20]A. B. Baggeroer, W. A. Kuperman, and H. Schmidt, "Matched field processing: Source localization in correlated noise as an optimum parameter estimation problem," J. Acoust. Soc. Am. **83**(2), 571–587 (1988).
[21]L. T. Fialkowski, J. S. Perkins, M. D. Collins, M. Nicholas, J. A. Fawcett, and W. A. Kuperman, "Matched-field source tracking by ambiguity surface averaging," J. Acoust. Soc. Am. **110**(2), 739–746 (2001).
[22]J. Murray and D. Ensberg, "The Swellex-96 experiment," http://swellex96.ucsd.edu/ (1996) (Last viewed May 2, 2023).
[23]M. Porter and E. L. Reiss, "A numerical method for ocean-acoustic normal modes," J. Acoust. Soc. Am. **76**(1), 244–252 (1984).
[24]M. B. Porter, "The KRAKEN normal mode program," Report No. SM-245, SACLANT Undersea Research Centre, La Spezia, Italy (1991).